Chaotic scattering in collinear Ze^-e^- three-body Coulomb systems

Bin Duan, Zaiqiao Bai, and Yan Gu
Department of Astronomy and Applied Physics, Center of Nonlinear Science, University of Science and Technology of China, Hefei, Anhui 230026, China

(Received 11 October 1999; published 17 May 2000)

We study the collinear chaotic scattering between an electron and a one-electron ion (e.g., He^+) with negative total energy. The global dynamics of the unbounded motion in phase space can be illustrated by introducing two submanifolds of critical injecting and critical escaping. We find a type of bifurcation of chaotic scattering resulted from the tangency between these two submanifolds, which explains the emergence or disappearance of an extra zeroth-order chaotic band in the scattering functions as the nuclear charge Z is changed.

PACS number(s): 34.80.Kw, 05.45.−a

The classical dynamics of three-body Coulomb systems is a long-standing problem of great physical importance. The first systematic attack on it, with the aim of understanding the spectrum of a helium atom, were carried out in the earlier period of the development of quantum mechanics [1]. However, those works totally failed because, as recognized today, the pioneers had no preparation for chaos at all. Even now, a thorough understanding of this high-dimensional nonintegrable system still remains a challenge for physicists equipped with knowledge of modern dynamical system theory. A practical strategy is to study the motions restricted on its low-dimensional invariant manifolds, which include among others, the coplanar motions [2,3], the e^-Ze^- and Ze^-e^- collinear motions [4–7], and the *s*-wave motions [8]. It is natural to expect that any knowledge of those subsystems will provide useful information about the original problem. In fact, the discovery of the stable bounded motions in the Ze^-e^- collinear helium [9,5] strongly supported the frozen planet model which has been used in explaining the highly correlated two-electron motions observed experimentally in doubly excited atoms or ions [10]. In this short paper we report our recent study on the unbounded motions, i.e., scatterings, in the Ze^-e^- collinear helium, noting that the scattering process explores the outer part of the phase space more thoroughly and that it will yield useful information about two-electron correlations in three-body Coulomb systems.

The Ze^-e^- collinear helium is composed of two electrons and one nucleus with charge Z. Both electrons are collinearly arranged on the same side of the nucleus, and since the nucleus is much heavier than the electron, the nucleus is supposed to be fixed at the origin. The Hamiltonian of the model is (in atomic units, $m_e=e=1$)

$$H=\frac{p_1^2}{2}+\frac{p_2^2}{2}-\frac{Z}{r_1}-\frac{Z}{r_2}+\frac{1}{r_1-r_2}, \tag{1}$$

where r_1 (or r_2) is the distance of the outer (or inner) electron from the nucleus with p_1 (or p_2) being its conjugate momentum. Since the potential is a homogeneous function of r_1 and r_2, the classical dynamics is invariant under a scaling transformation with respect to the total energy E. Thus it is sufficient to perform calculations at the fixed energy $E=-1$ for the negative total energy.

The best way to study the collinear helium dynamics is using the Poincarè surface of section (SOS), where an orbit can be conveniently visualized by its points of intersection with a two-dimensional SOS. The bounded motions of a Ze^-e^- collinear helium were shown in Fig. 8 of Ref. [5], and they are hardly distinguishable from an integrable system. The fundamental periodic orbit of the system appears as a fixed point in the center of an extended torus structure. Near the fixed point, the motion of the outer electron is nearly harmonic, while for large radial distances the tori are elongated due to the almost Keplerian motion of the outer electron. However, with the increase of Z, the KAM tori break up one by one, and the chaotic motion is expected to appear. For the scattering orbits, we can classify them into direct and resonant ones. The direct scattering orbits, which lead to the immediate escape of the outer electron after an *e*-*e* collision, are topologically the same as there in Coulomb potential scattering. On the other hand, in a resonant scattering orbit, the outer electron, which fails to escape to infinity during its first outgoing phase, will experience an indefinite number of reinjecting phase and lead to a very complex trajectory. In the following, we will focus our attention on the characteristics of the resonant scatterings of Ze^-e^- collinear helium.

We shall first explain in some detail our considerations on the numerical calculations. Since the resonant scatterings can only be observed in injecting ensembles with an incident energy slightly above zero, it would be very time consuming to directly use the exact dynamical equations in numerical studies. To circumvent this difficulty, we divide the position of the outer electron into three zones by setting two radii r_a and r_b. The asymptotic zone is defined by $r_b<r_1$ where the correlation between the two electrons can be neglected so that the mean-field approximation is justified. Specifically, the Hamiltonian can be separated into two parts, i.e., $H=H_1+H_2$, for the inner and outer electrons as

$$H_2=\frac{p_2^2}{2}-\frac{Z}{r_2} \tag{2}$$

and

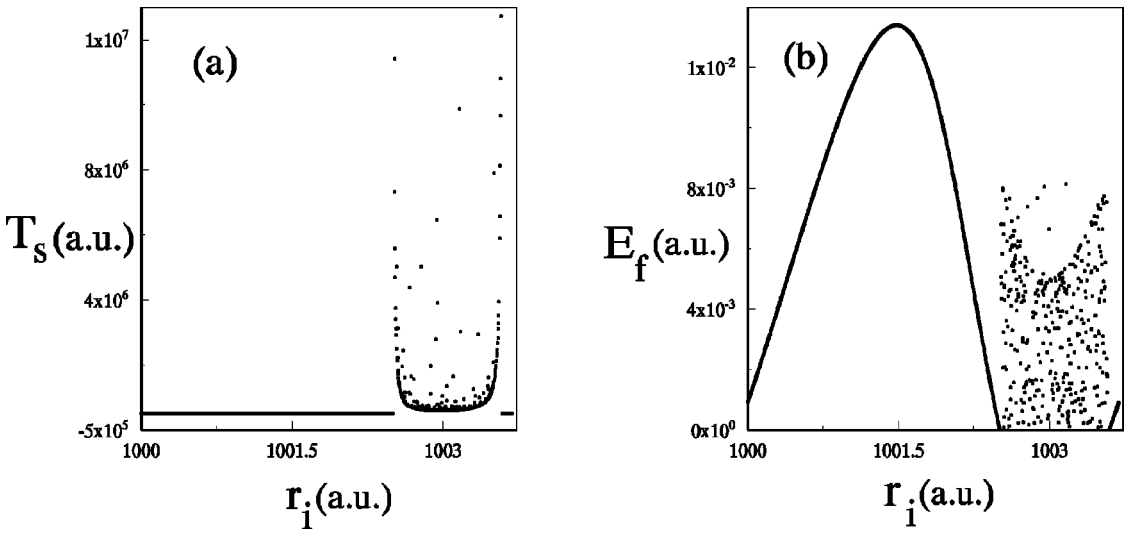

FIG. 1. Scattering functions for $Z=10$ and $E_i=0.005$ (full range). (a) Scattering time T_s, (b) escaping energy E_f.

$$H_1=\frac{p_1^2}{2}-\frac{Z}{r_1}+\frac{1}{r_1-\langle r_2\rangle}, \tag{3}$$

where $\langle r_2\rangle=-0.75Z/H_2$ is the time average of r_2 in a period of e_2 [11]. Therefore, an analytical result can be obtained in this asymptotic zone. In the middle zone defined by $r_a<r_1<r_b$, H_2 remains almost constant but the e-e correlation is no longer negligible. In this region we rewrite the dynamical equations by using (θ,I), the angle action of H_2, and treat I as a slow variable so that a large step integrator can be applied. Finally, $r_1<r_a$ defines the e-e strongly interacted zone, where the above method may fail. In this zone, we use exact dynamical equations with a regularization of two-body collision. For our purposes, we have found that a choice of $r_b\approx 100Z$ and $r_a\approx 5Z$ in our numerical code can conserve the energy to within 10^{-6} for most of the trajectories we shall report below.

With the above explanation of the computational methods, we now turn to the description of numerical scattering experiments. We first prepare a complete injecting ensemble in which the inner electron is fixed at the origin with $H_2=-1-E_i$ while the outer electron is uniformly distributed within a range of $r_1=r_i\in[r_b,r_b+\Delta r)$ with $H_1=E_i$, and Δr being the distance that the outer electron travels during a period of the inner electron. Taking each member of the injecting ensemble as an initial point, we compute its orbit until the outer electron fulfills the escaping condition given by $p_1>0$, $H_1>0$, and $r_1>r_b$. The records of the escaping energy E_f and scattering time T_s as a function of the initial parameter r_i yield the scattering functions.

The scattering functions for a complete injecting ensemble with $E_i=0.005$ and $Z=10$ are shown in Fig. 1, from which we can see the hierarchical self-similar structure, the signature of the chaotic scattering. Figure 1 shows that the

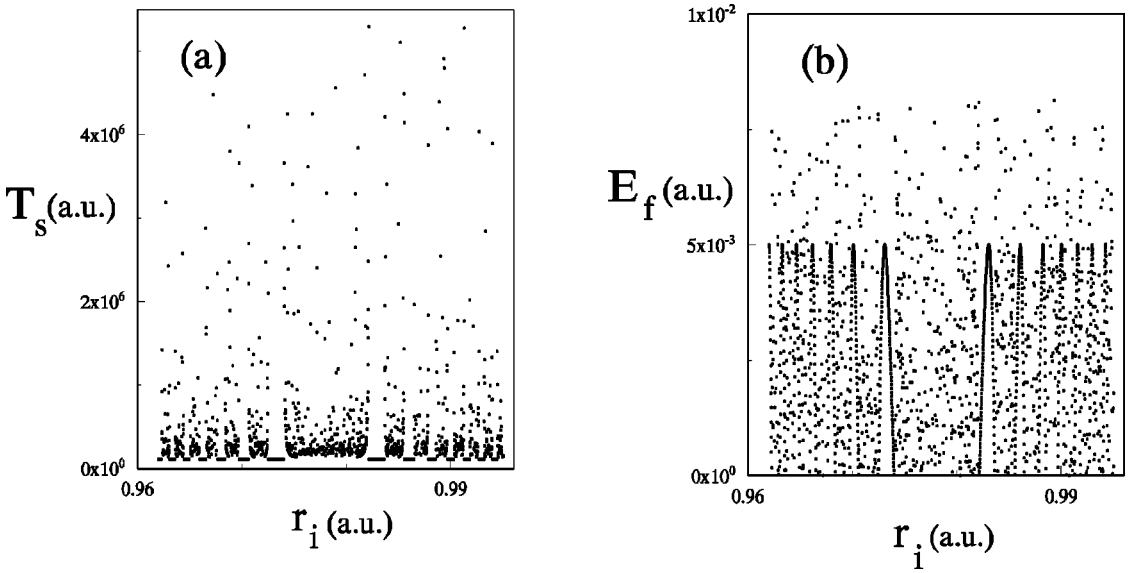

FIG. 2. Blowup of the central part of the chaotic band in Fig. 1, the abscissa is indicated as r_i-1002. (a) Scattering time T_s, (b) escaping energy E_f.

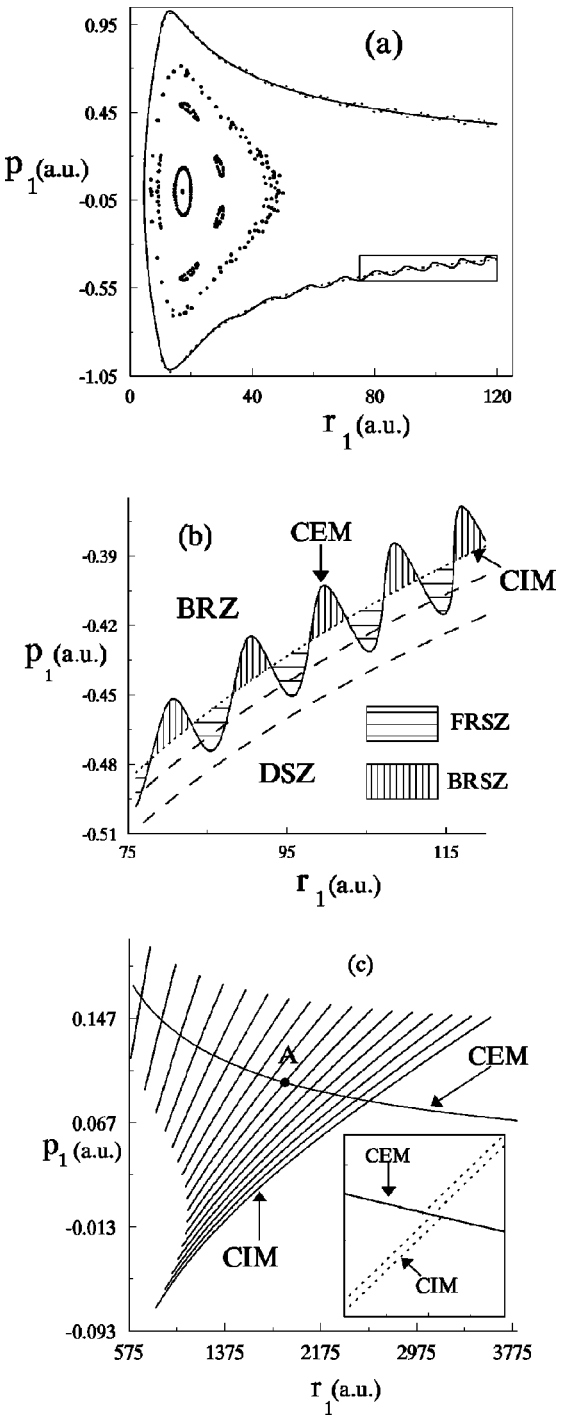

FIG. 3. (a) Phase portrait of the SOS for some bounded orbits and a part of the CEM (solid line) and the CIM (dotted line) when $Z=10$. (b) Enlargement of the rectangle in Fig. 2(a). The CEM (solid line), CIM (dotted line), and two ensembles (dashed lines) with $E_i=0.005$ (upper) and $E_i=0.012$ (lower) are plotted. The FRSZ and BRSZ are marked out by shaded regions while the blank regions below and above the CIM denoted direct scattering and biresonant zones, respectively. (c) Propagation of the oscillated CIM in the asymptotic zone. Trajectories of a complete injecting ensemble are plotted by stroboscopic sampling at a period of 50 cycles. The inset in the figure shows the enlargement of the region in the vicinity of the point A.

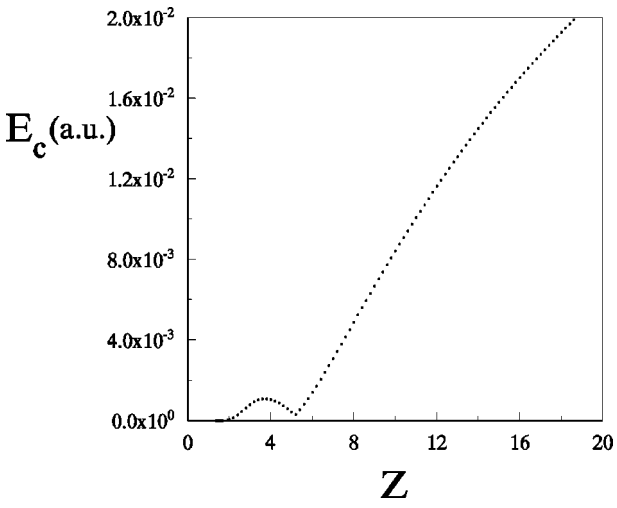

FIG. 4. Threshold E_c as a function of Z.

scattering functions consist of regular and irregular components. In the regular part, which we call the zeroth-order regular band, E_f and T_s are continuous with respect to r_i. On the contrary, the scattering functions violently fluctuate in the irregular part, which we call the zeroth-order chaotic band.

If we enlarge the zeroth-order chaotic band, a finer structure will appear (Fig. 2). We can see that the chaotic band consists of infinitely many interlaced regular parts and fluctuating parts, which are called the first-order regular bands and chaotic bands, respectively. Each regular band is a concave parabola for T_s, and a convex parabola for E_f. Moving away from the central and widest chaotic band, the width of the regular bands and chaotic bands gradually shrink to zero as they approach the borderline of the zeroth-order chaotic band. Further enlargement of a first-order chaotic band reveals a similar picture, i.e., (the second-order) regular bands separated by (the second-order) chaotic bands. As we will discuss later, this hierarchical self-similar structure can actually be observed in an arbitrary fine scale, which indicates the existence of chaotic scattering in Ze^-e^- collinear helium.

To understand the onset of chaotic scattering, we will study the global dynamics of the system on the SOS. We choose the SOS as the phase plane $\{r_1,p_1\}$ of the outer electron when the inner electron is at its aphelion (i.e., $p_2=0$). A typical phase portrait on the SOS is shown in Fig. 3(a). By introducing the critical escaping and injecting manifolds on the SOS, orbits with qualitatively different behavior can be clearly identified. Consider the orbits starting from the SOS's with different $p_1>0$ and fixed r_1. They can be classified into either of the following three types according to the fate of the outer electron. If p_1 is sufficiently large, the outer electron will immediately escape to infinity with finite outgoing energy. On the other hand, if p_1 is not large enough, the outer electron will return to the vicinity of the nucleus due to the (time-dependent) attractive potential. In addition to these two general situations, there exists a critical case when the outer electron directly escapes with zero energy. The intersections

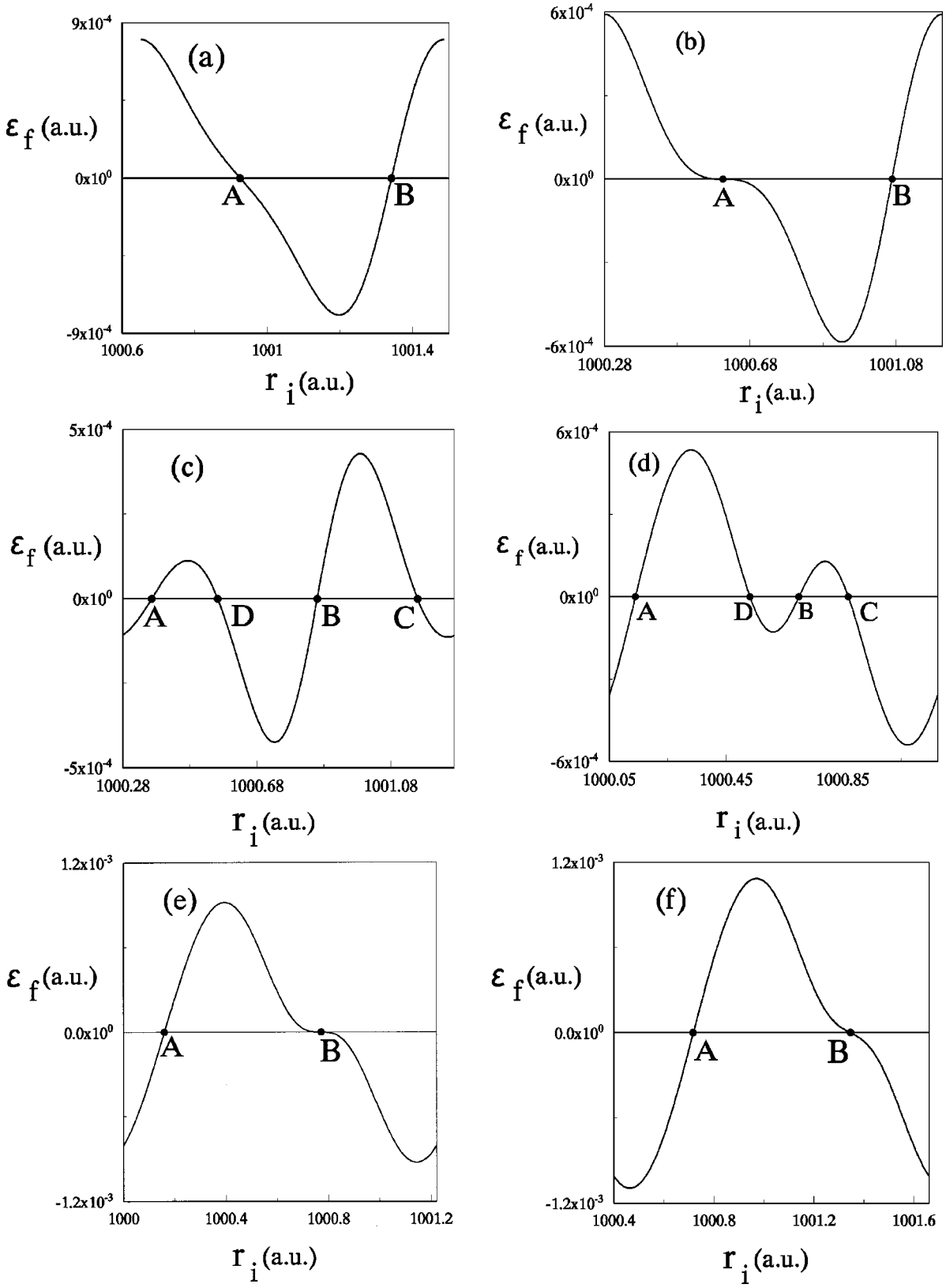

FIG. 5. ε_f function. (a) $Z=4.5$; (b) $Z=Z_1$; (c) $Z=5.0$; (d) $Z=5.4$; (e) Z=Z2; (f) $Z=5.8$. *Note that the relative position of the zeroth-order chaotic band with respect to points A* and *B* is changed after the transition [see (a) and (f)].

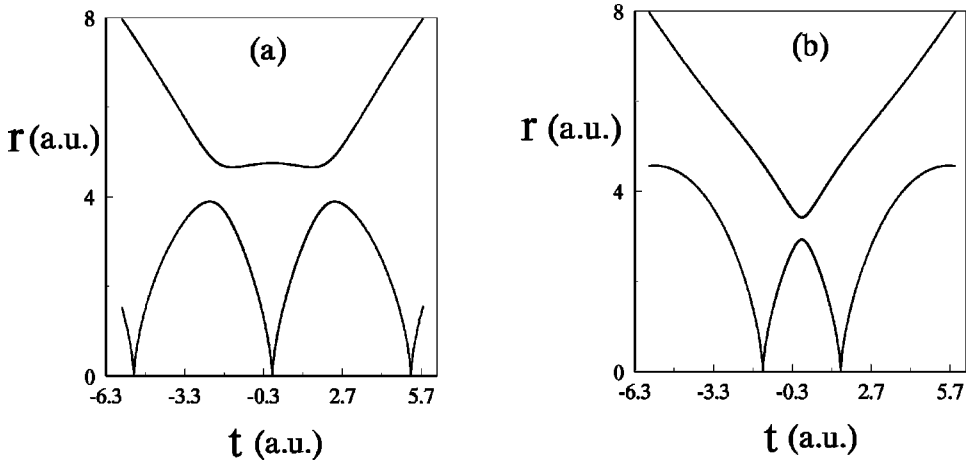

FIG. 6. Two symmetric RCO's at $Z=4.7$.

of these critical escaping orbits with SOS define a curve, which we shall call the critical escaping manifold (CEM). By applying the time reversal transformation ($p_1 \rightarrow -p_1$) to the CEM, we obtain the critical injecting manifold (CIM). In numerical studies, the CIM can be generated by an injecting ensemble with nearly zero incident energy.

The geometrical locus of the CIM (or the CEM) on SOS is in general very complicated. However, the initial (or final) part of the CIM (or CEM) is relatively smooth and has the axis $p_1=0$ as its asymptote when $t \rightarrow -\infty$ (or $t \rightarrow +\infty$). In Fig. 3(a) we have plotted out these primitive parts of CIM and CEM for the $Z=10$ system. Noting that the CIM (or CEM) is the separatrix between the regions of direct injecting (or escaping) and reinjecting (or resonant) orbits, we can use them to classify the SOS into four zones: (i) direct scattering zone (DSZ), (ii) forward resonant scattering zone (FRSZ), (iii) backward resonant scattering zone (BRSZ), and (iv) biresonant zone (BRZ). It is obvious that the bounded orbits form a subset of the BRZ which is invariant under the time evolution (i.e., under Poincaré mapping), while the re-

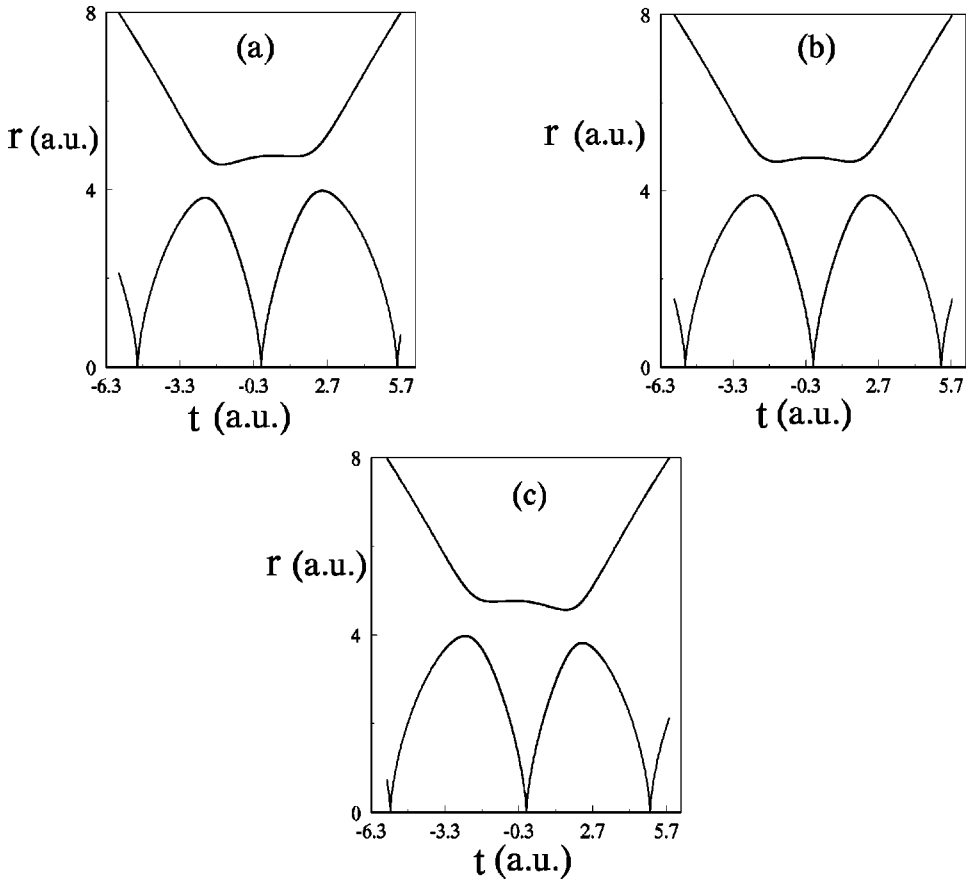

FIG. 7. Two newborn asymmetric RCO's (C and D) when $Z=4.8$ together with the symmetric one (A), from which they are bifurcated.

maining points in the BRZ as well as the points in the FRSZ will eventually fall into the BRSZ and escape to infinity. Thus these remaining points in the BRZ plus the points in the FRSZ and BRSZ represent all the resonant scattering orbits. Figure 3(b) shows an enlargement of the rectangle region in Fig. 3(a), which clearly displays the partition of regions for orbits with different global behaviors. It should also be noted that for a finer classification of resonant scattering orbits, it is necessary to propagate the CIM further so that it exhibits wild oscillations [see Fig. 3(c)]. These oscillating segments of the CIM could extend back to the vicinity of the nucleus and result in secondary intersections with the CEM which generates a finer partition of the SOS.

Now we are ready to discuss the onset of the chaotic scattering with variations of the incident energy E_i. Two segments of incident ensembles with $E_i=0.012$ and 0.005 are shown in Fig. 3(b). Since the lower segment does not intersect with the CEM and is totally confined within the DSZ, all its orbits will directly escape and no chaotic scattering can be observed. While the upper one cuts the CEM and, consequently, the orbits located within the FRSZ will reinject after their outgoing phase. These resonant scattering orbits lead to the zeroth-order chaotic band in the scattering functions. Since all the orbits within FRSZ will undergo a Keplerian excursion and reinject from the large r_1 region, a finer structure of the zeroth-order chaotic band will be generated by ''secondary scatterings with negative incident energy.'' Just as in the original scattering, an orbit in the secondary scatterings will either directly escape, if it falls into the BRSZ after the first excursion, or reinject once more if it falls into the BRZ. The same story repeats itself *ad infinitum* which explains the self-similarity of the scattering functions.

Based on the above discussions we conclude that chaotic scattering can only occur if E_i is less than a (Z-dependent) threshold E_c, where the incident ensemble is tangent to the CEM. Furthermore, we can see that the resonant width D_r (which is defined as the portion of the resonant orbits in a complete injecting ensemble) obeys the square root law near E_c, i.e., $D_r \propto (E_c - E_i)^{1/2}$. In order to evaluate the value of E_c, we can prepare a critical injecting ensemble and compute the energy ε_f [expressed by Eq. (3)] of the outer electron when it attains the asymptotic region during its first outgoing phase. In contrast with the scattering function E_f, the energy ε_f as a function of the initial parameter r_i is smooth which coincides with E_f in its zeroth-order regular band and takes negative values in the zeroth-order chaotic band of E_f. Since the numerical calculations of ε_f are much easier than that for E_f, it is convenient to use ε_f instead of E_f in the study of the zeroth-order structure of the scattering functions. The threshold energy E_c, which characterizes the emergence of chaotic scattering, can be simply read as the maximum of ε_f.

The threshold E_c as a function of Z is shown in Fig. 4, from which we can see two remarkable features. First, E_c nearly vanishes ($<10^{-10}$) if $Z<Z_0\approx 1.534$. We are not sure whether the CEM coincides exactly with the CIM in this case. This seems to suggest that the system is integrable if $Z<Z_0$, and this is supported by our observation on the phase portrait of the bounded motions also.

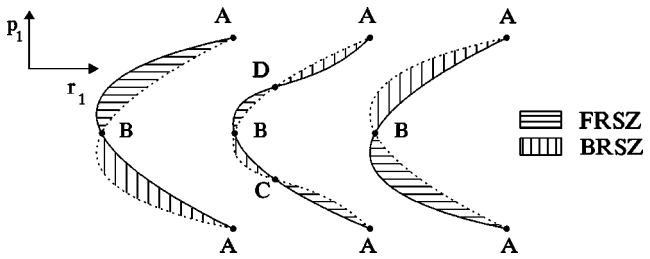

FIG. 8. Schematic diagram showing the transition of the CIM (dotted line) and the CEM (solid line). The three situations from left to right represent the cases of $Z<Z_1$, $Z_1<Z<Z_2$, and $Z>Z_2$, respectively.

Secondly, although E_c is, mostly, a monotonously increasing function of Z, it exhibits a deep dip near $Z=5.2$. To find out what happens in this region, the ε_f functions with $Z=4.5$, 4.7938, 5, 5.4, 5.684, and 5.8 are plotted in Fig. 5, from which we can see two apparent transitions, i.e., a V-shaped ε_f function changes to a W-shaped one and turns back (noting that ε_f is defined on a circle). Let us focus on the former transition which occurs at $Z=Z_1\approx 4.7938$. If $Z<Z_1$, the ε_f function has two zero points A and B. Each zero point of the ε_f function corresponds to a distinct direct scattering orbits with both incident and escaping energies equal to zero, which we shall call a reversible critical orbit (RCO). On the SOS, a RCO is represented by a sequence of points where the CIM meets the CEM. By using the time reversal symmetry, we can declare that there exist at least two (time-reversal) symmetric RCO's which are characterized by $r_2=0$ and $p_2=0$, respectively, when the outer electron is stopped in the vicinity of the nucleus. Therefore A and B must represent two symmetric RCO's. Specifically, the point $A(B)$ corresponds to the one with $r_2=0(p_2=0)$ when $p_1=0$ (Fig. 6).

When $Z=Z_1$, $d\varepsilon_f/dr_i$ vanishes at point A [Fig. 5(b)], which causes a bifurcation of the zero points of the ε_f function. Geometrically, it is manifested by the tangency between the CIM and the CEM at the corresponding points. If Z passes this point, two additional zero points appear [C and D in Fig. 5(c)], which correspond to two asymmetric RCO's [Fig. 7]. An important physical consequence of this bifurcation is that a new zeroth-order chaotic band will be observed if the incident energy is sufficiently small. With the increase of Z, the two new-born zero points depart gradually and at $Z=Z_2\simeq 5.684$ they collide with the point B and disappear [Fig. 5(e)]. This is the inverse transition of the former one. After the second bifurcation, the zeroth-order chaotic band will again consist of one piece.

From a topological point of view, the two symmetric RCO's are connected through the production and annihilation of the asymmetric RCO pair. This can cause an important global effect. Geometrically, when Z runs from Z_1 to Z_2, the two critical manifolds approach and cross each other and, consequently, their relative location is actually exchanged (Fig. 8). Since E_c characterizes, in a sense, the width of the region enclosed by the CIM and the CEM, the crossing of

these two manifolds can explain the observed decrease of E_c during the transitions.

In conclusion, our investigations show that the one-dimensional Ze^-e^- system is chaotic when $Z>Z_0\approx 1.534$. For such two-electron systems, chaotic scattering (or chaotic autoionization) will occur in a prescribed energy regime as shown in Fig. 4. It is expected that these results will provide necessary information for understanding the quantum manifestations of classical chaos in real two electron-systems.

This work was supported by the Nonlinear Science Project of the Climbing Program for Fundamental Research.

[1] M. Born, *Vorlesungen über Atommechanik* (Springer, Berlin, 1925) [English translation, *The Mechanics of the Atom* (Ungar, New York, 1927)].

[2] Y. Gu and J.M. Yuan, Phys. Rev. A **47**, R2442 (1993); J.M. Yuan and Y. Gu, Chaos **3**, 569 (1993).

[3] T. Yamamoto and K. Kaneko, Phys. Rev. Lett. **70**, 1928 (1993).

[4] D. Wintgen, K. Richter, and G. Tanner, Chaos **2**, 19 (1992).

[5] K. Richter, G. Tanner, and D. Wintgen, Phys. Rev. A **48**, 4182 (1993).

[6] X. Tang, Y. Gu, and J.M. Yuan, Phys. Rev. A **54**, 496 (1996).

[7] Z.Q. Bai, Y. Gu, and J.M. Yuan, Physica D **118**, 17 (1998).

[8] G. Handke, M. Draeger, W. Ihre, and H. Friedrich, Phys. Rev. A **48**, 3699 (1993); G. Handke, *ibid.* **50**, R3561 (1994).

[9] K. Richter and D. Wintgen, Phys. Rev. Lett. **65**, 1965 (1990).

[10] U. Eichmann, V. Lange, and W. Sandner, Phys. Rev. Lett. **64**, 274 (1990).

[11] Strictly speaking, the effective e-e interaction in H_1 should be $\langle 1/(r_1-r_2)\rangle$, which can be easily evaluated (by substituting $r_2=a\sin^2\varphi$ and $p_2=\sqrt{-2H_2}\cot\varphi$ with $a=-Z/H_2$) and read $2/(r_1-a+\sqrt{r_1(r_1-a)})$. However, as $2/(r_1-a+\sqrt{r_1(r_1-a)})=1/(r_1-\langle r_2\rangle+a^2/16r_1+\cdots)$, our choice of H_1, which is more convenient than the strict one in calculation, will be a good approximation if r_b is sufficiently large.